HYDROLOGICAL PROCESSES
Hydrol. Process. **21**, 2623–2640 (2007)
Published online in Wiley InterScience
(www.interscience.wiley.com) DOI: 10.1002/hyp.6793

Determining snow water equivalent by acoustic sounding

N. J. Kinar and J. W. Pomeroy*
Centre for Hydrology, University of Saskatchewan, Saskatoon, Canada

Abstract:

The possibility of determining snow water equivalent (SWE) by the use of an acoustic impulse was assessed at two field locations in Saskatchewan and British Columbia, Canada. These sites represent cold windswept prairie and temperate deep mountain snowcovers. A continuous frequency-swept acoustic wave was sent into the snowpack and received. Signal processing was then subsequently used to estimate the depth and density of each snow layer by a recursive relationship involving frequency-modulated continuous-wave (FMCW) radar and seismological techniques. From this method, it is also shown that the tortuosity of snow can be estimated. Data collected by gravimetric sampling was used as comparison to the SWE values determined by the use of acoustic sounding. The results showed that for the Saskatchewan sites, the correlation between the measured and the modeled values of SWE was 0·86, whereas at the British Columbia sites, the correlation was 0·78. The difference in the correlations was interpreted as being due to additional acoustic measurement error at the British Columbia sites caused by higher liquid water contents and more layers in the snowpack. The measured and the modeled SWE for Saskatchewan snowpacks with high liquid water contents were found to be weakly associated with correlations of 0·30. The acoustically-determined values of tortuosity were close to unity ($\alpha \approx 1$), which is in agreement with the values characteristic of snow as a porous substance. Further research is necessary to determine whether this technique can be applied to snow in other environmental conditions. Copyright © 2007 John Wiley & Sons, Ltd.

KEY WORDS snow; sound; snow water equivalent; acoustics; snow measurement; Saskatchewan; British Columbia; prairie snowpack; mountain snowpack

Received 1 June 2006; Accepted 28 December 2006

INTRODUCTION

Snow water equivalent (SWE) is generally determined by the use of invasive devices that involve physical modification of the snowpack. For example, snow depth is found by inserting a graduated rod into the snowpack. Snow density is estimated by the use of gravimetric sampling, which involves the extraction and weighing of samples from a layered snowpack. Gravimetric sampling can be conducted either by the use of a scoop that is used to extract snow from the side of a snowpit (Woo, 1997), or by a snow tube inserted vertically to extract a core from the snowpack (Bindon, 1964).

These physical methods of determining SWE, although capable of giving adequate estimates of snow depth or density, have a number of caveats that are described by Pomeroy and Gray (1995). Despite the fact that instruments such as the scoop sampler or the snow tube have enjoyed widespread use, snow surveying for the determination of SWE is a labourious task i.e. time-consuming, expensive, tedious and prone to human error. Recent snow measurement research has focused on the development of frequency-modulated continuous-wave (FMCW) radar to determine snow depth or density (Gubler and Hiller, 1984; Koh *et al*., 2002; Marshall *et al*., 2004; Yankielun *et al*., 2004) however such a procedure is not entirely non-invasive. FMCW radar techniques have shown utility in estimating snow depth or density, but not both. Additional measurements of a quantity such as snow density are usually required. Moreover, neither snow depth nor density alone can determine SWE; both of these quantities are needed to adequately estimate SWE. Snow depth at a fixed location has been determined in a non-invasive fashion by the use of a sensor which measures the return time of an acoustic pulse to find the distance to the top of the snowpack (Gubler, 1981; Goodison *et al*., 1984; Goodison *et al*., 1988). Although empirical relationships have been derived that relate the depth of snow to SWE, the use of these relationships is usually limited to one geographic area (Pomeroy and Gray, 1995).

Experiments with the use of an acoustic pulse were conducted with the objective of advancing the determination of SWE in a non-invasive manner. The intention was to use theoretical aspects of FMCW radar (Luck, 1949; Stove, 1992) and digital signal processing to aid in a novel analysis of the acoustic pulses and thereby determine snow depth and density, the two required quantities for an estimate of SWE. Such an approach builds upon the established literature associated with the investigation of sound propagation in snow (Oura, 1952a,b; Smith, 1965; Smith, 1969; Bogorodskii *et al*., 1974; Johnson, 1982; Cummings and Holliday, 1983; Sommerfeld, 1982; Zhekamukhov and Malkandueva, 2004) and the important conclusions made by Johnson (1982), Lee and Rogers (1985), Attenborough and Buser (1988), Moore

* Correspondence to: J. W. Pomeroy, Centre for Hydrology, University of Saskatchewan, 117 Science Place, Saskatoon, Sask., S7N 5C8, Canada. E-mail: pomeroy@usask.ca

et al. (1991), and Albert (2001) that sound can be successfully used to determine the physical properties of the snowpack.

THEORY

Model

To establish a conceptual model of the snowpack system, the snowpack is assumed to be a porous medium consisting of an elastic framework that is saturated with air. Such an assumption was made by Johnson (1982), who used the theory of Biot (1956a,b) to describe the propagation of sound in snow. Moreover, it is assumed (Johnson, 1982) that three types of sound waves (two dilatational waves and one shear wave) are present in the snowpack. Dilatiational and shear waves in snow were independently recognized by Zhekamukhov and Malkandueva (2004) as longitudinal and transverse disturbances. The two dilatational waves have a compressional motion. The first dilatational wave travels in the ice matrix of the snowpack, but the second wave is a strongly-attenuated air pressure disturbance that propagates in pore spaces. Both waves are coupled, in that there is transfer of motion between the air spaces and the ice matrix of the snowpack. The phase velocity of the first dilatational wave is often higher than the phase velocity of the second dilatational wave (Albert, 1993a), but it is possible for either the first or the second dilatational wave to travel faster or slower than the other. Because of this, the first dilatational wave is referred to as the 'fast wave', whereas the second dilatational wave is considered to be the 'slow wave'. We are primarily interested in the slow dilatational pressure wave that travels in the pore spaces of the snowpack. This is because the Biot theory predicts that most of the energy from an air wave incident on an air-filled porous medium such as snow will be transmitted to the pore spaces, and therefore, the energy of the first dilatational wave and the shear wave will be negligible (Moore *et al*., 1991; Albert, 1993b).

The snowpack is assumed to consist of a series of N layers $\{L_1, \ldots, L_N\}$, where $\{\Omega_1, \ldots, \Omega_N\}$ are the interfaces between the layers (Figure 1(a)). The interfaces are introduced as a conceptual construct and are assumed to be massless. Although it is conceivable that a velocity gradient might exist within some of the layers due to gradual changes in physical properties with increasing depth in the same manner as a layered earth (i.e. Kennett, 2001), it is assumed that the kinematics of a sound wave

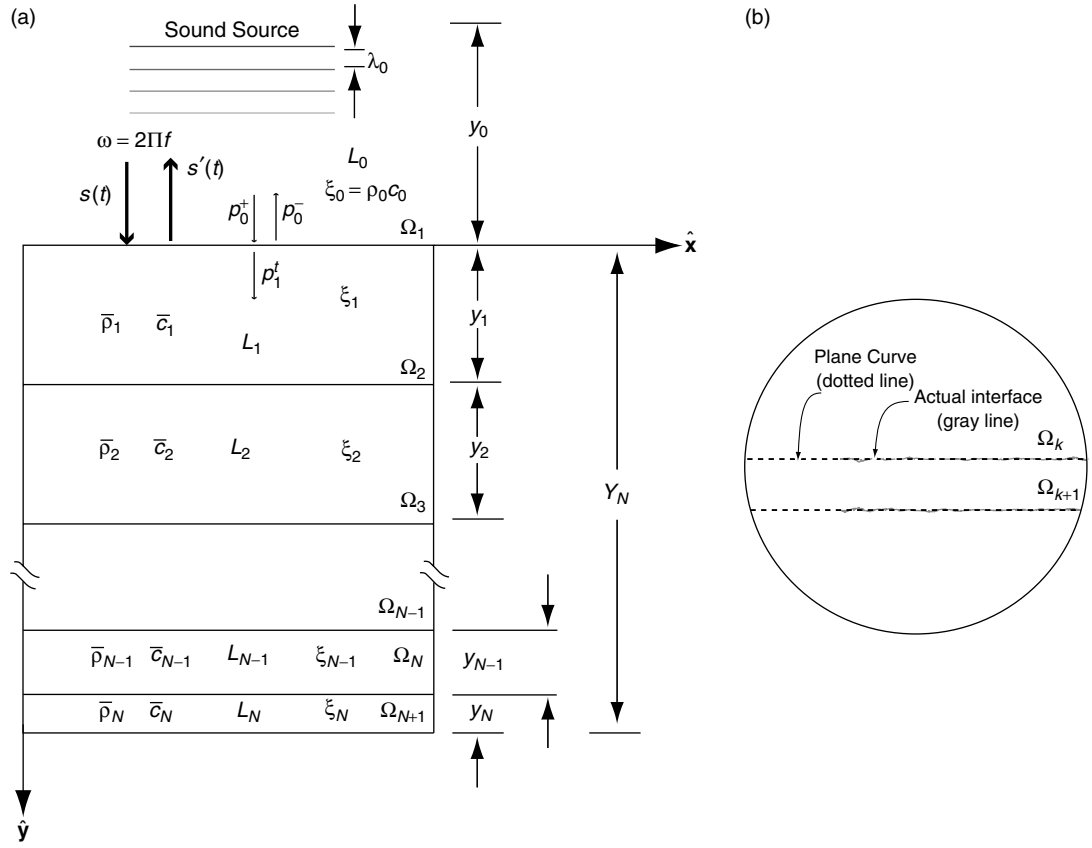

Figure 1. Conceptual diagram of the snowpack system. The wavelength of the sound source in the air layer L_0 above the surface of the snowpack is λ_0; the distance from the source to the surface of the snowpack is y_0; the acoustic impedance of the air layer is ξ_0; the acoustic impedance of the layers of the snowpack is $\{\xi_1, \ldots, \xi_N\}$; the equilibrium density of the air layer is ρ_0; the phase velocity of the sound wave in the air layer is c_0; the angular frequency of the plane wave source is ω; the frequency of the source is f; the original sound wave sent from the source is expressible as the continuous function $s(t)$; the overall reflection from the snowpack is $s'(t)$; the pressure of the acoustic wave arriving at the first interface of the snowpack is p_0^+; the pressure of the reflected wave is p_0^-; the pressure of the transmitted wave across the interface Ω_1 at the surface of the snowpack is p_1^t; the density and speed of an acoustic impulse in a given layer L_k of the snowpack is $\overline{\rho}_k$ and $\overline{c}_k$, respectively; the vertical dimension of each of the layers is $\{y_0, \ldots y_N\}$, and the total cumulative depth of the snowpack is Y_N

DOI: 10.1002/hyp

through the snowpack at normal incidence to the first interface Ω_1 is describable by the average phase velocity $\overline{c}_k$ in a specific layer L_k as it travels over the vertical dimension of the layer. Even if the phase velocity of the wave gradually changes over depth, it is impossible in the context of this experiment to obtain physical properties of the layers until there is a reflection of the pressure wave. This is what is referred to in reflection seismology as the 'inverse problem'. The interface between two layers of the snowpack is assumed to be a plane curve that represents the best-fit surface of the actual (undulating or rough) interface (Figure 1(b)). Although such a definition is not precise it strongly implies that an acoustic pressure wave travelling through the snowpack will be reflected at the interface between two layers due to a change in acoustic impedance ξ_k.

Consider an acoustic pressure wave with an angular frequency ω that originates in air at a height of y_0 above the surface of the snowpack. The air layer above the snowpack is considered to be layer L_0 in this physical system (Figure 1(a)). Assume that the wave radiates toward the snowpack in a positive direction that is perpendicular to the snow surface and parallel to the $\hat{\mathbf{y}}$-axis of the coordinate system. The distance y_0 is assumed to be sufficiently large such that when the pressure wave reaches the snow surface Ω_1 it can be assumed to be planar. The pressure fluctuations in the air layer above the snowpack transfer momentum to the snow structure and to the air in the pore spaces of the snow by means of acoustic-to-seismic coupling (Albert, 1987; Albert and Orcutt, 1989; Albert and Orcutt, 1990; Albert, 1993a). Owing to an impedance mismatch between the air and snow, the wave is reflected at the boundary. The boundary conditions for the pressure wave at the air-snow interface are:

$$p_0^+ + p_0^- = p_1^t \tag{1}$$

$$c_0^+ + c_0^- = p_1^t \Leftrightarrow (p_0^+/\xi_0) + (p_0^-/\xi_0) = (p_1^t/\xi_0) \tag{2}$$

where the pressure of the air wave approaching the snow surface is p_0^+, the pressure of the reflected wave is p_0^-, the pressure of the wave that is transmitted into the snowpack is p_1^t, and the nomenclature is similarly defined for the phase velocity in the air layer. We assume that Equations (1) and (2) are approximations when the sound source is situated at small angles to a line that is taken to be normal to the surface of the snowpack. Further research could be conducted to ascertain the effects of small angular deviation on the results of this method.

Dividing Equation (1) by p_0^+ and recalling that the effective pressure reflection coefficient is defined by the ratio $\Gamma_1 = p_0^-/p_0^+$, it follows that:

$$\Gamma_1 = \frac{\xi_1 - \xi_0}{\xi_1 + \xi_0} \tag{3}$$

The next step is to find expressions for the acoustic impedances of air and snow.

Estimation of the acoustic impedance of a snow layer requires a measure of the tortuosity, which can be defined as the deviation from a straight line of a path through the connected pore space in a porous medium. Johnson *et al.* (1987) demonstrated that their theory is an extension of the work of Biot (1956a,b) and therefore the constituent equations of the Biot theory can be taken as a special case. They conclude that their expression for the dynamic tortuosity $\alpha(\omega)$ can be applied in general to a fluid-saturated porous medium with an elastic framework. Building on the research of Johnson *et al.* (1987), Champoux and Allard (1991), and Lafarge *et al.* (1997), it was recognized by Umnova *et al.* (2005) that the real-valued acoustic impedance of a porous medium is:

$$\xi_1 = \frac{\rho_0 c_0 \sqrt{\alpha(\omega)}}{\phi} \tag{4}$$

Note that Equation (4) is not normalized with respect to the characteristic impedance of air. Returning to Equation (3), it follows that:

$$\Gamma_1 = \frac{\rho_0 c_0 \sqrt{\alpha_1(\omega)} - \phi \rho_0 c_0}{\rho_0 c_0 \sqrt{\alpha_1(\omega)} - \phi \rho_0 c_0} \tag{5}$$

and,

$$\phi_1 = \sqrt{\alpha_1(\omega)} \left(\frac{1 - \Gamma_1}{1 + \Gamma_1} \right) \tag{6}$$

Equation (6) is also given by Umnova *et al.* (2005). An implicit assumption of Equation (6) is that the porosity of the first snow layer can be calculated without knowledge of the characteristic acoustic impedance $\rho_0 c_0$ of the air layer above the snowpack or the acoustic impedance of the air-filled pore spaces of the snowpack.

Although snow is a dispersive (lossy) medium that strongly attenuates sound, it is assumed that the pressure wave travels through snow until a change in impedance is significant enough to cause a reflection at the interface Ω_2 between two layers L_1 and L_2 of the snowpack. Taking boundary conditions once again at this interface, the effective reflection coefficient is given by:

$$\Gamma_1 = \frac{\xi_2 - \xi_1}{\xi_2 + \xi_1} \tag{7}$$

$$\Gamma_1 = \frac{\phi_1 \rho_0 c_0 \sqrt{\alpha_2(\omega)} - \phi_2 \rho_0 c_0 \sqrt{\alpha_1(\omega)}}{\phi_1 \rho_0 c_0 \sqrt{\alpha_2(\omega)} + \phi_2 \rho_0 c_0 \sqrt{\alpha_1(\omega)}} \tag{8}$$

$$\phi_2 = \frac{\phi_1 \sqrt{\alpha_2(\omega)}}{\sqrt{\alpha_1(\omega)}} \left(\frac{1 - \Gamma_2}{1 + \Gamma_2} \right) \tag{9}$$

Assuming that the wave continues travelling through the snowpack, it will be reflected at each successive boundary Ω_k until the energy in the pressure disturbance of the medium is dissipated. Thus, generalizing Equation (9) for a particular boundary k:

$$\phi_k = \frac{\phi_{k-1} \sqrt{\alpha_k(\omega)}}{\sqrt{\alpha_{k-1}(\omega)}} \left(\frac{1 - \Gamma_k}{1 + \Gamma_k} \right) \tag{10}$$

Equations (6) and (10) represent a means of calculating the porosity of a snow surface, given the dynamic tortuosity $\alpha_k(\omega)$ of each layer and the effective reflection

DOI: 10.1002/hyp

coefficient Γ_k at the interface Ω_k between an air layer and a snow layer, or between a snow layer and another snow layer. It is assumed that the average porosity ϕ refers to the air-connected pore spaces in snow, following Moore *et al*. (1991) and Buser (1986). Both equations involve two variables expressible as the set $\{\phi_k, \alpha_k(\omega)\}$. A relationship between these two variables, the porosity ϕ_k of a porous medium and the tortuosity α_k, was found by Berryman (1980) as a consequence of the Biot theory. Berryman (1980) noted that:

$$\alpha_k = 1 - \gamma\left(1 - \frac{1}{\phi}\right) \tag{11}$$

where γ is a shape factor dependent on the geometry of the particles comprising the porous medium. Berryman (1980, 1983) has proven that $\gamma = 1/2$ for spherical particles; alternately, Johnson and Sen (1981) have found that $\gamma = 3/4$ for randomly-oriented particles with a needle-like geometry. A later section of this paper will present a sensitivity analysis of the model to variations in γ.

Substituting Equation (11) into Equations (10) and (6) yields two functions $\Phi(\Gamma_1, \phi_1) = 0$ and $\Phi(\Gamma_k, \phi_k) = 0$ that allow for the porosity of a layer L_k of the snowpack to be estimated by an iterative process, given a fixed numerical value for the effective reflection coefficient Γ_k:

$$\Phi(\Gamma_1, \phi_1) = \left(\frac{\phi_1 - \gamma\phi_1 + \gamma}{\phi_1}\right)^{1/2} - \frac{\phi_1(1+\Gamma_1)}{1-\Gamma_1} = 0 \tag{12}$$

$$\Phi(\Gamma_k, \phi_k) = \frac{\phi_{k-1}}{\sqrt{\alpha_{k-1}(\omega)}} \times \left(\frac{\phi_k - \gamma\phi_k + \gamma}{\phi_k}\right)^{1/2} - \frac{\phi_k(1+\Gamma_k)}{1-\Gamma_k} = 0 \tag{13}$$

The acoustic source is assumed to radiate plane waves parallel to the $\hat{\mathbf{y}}$-axis of the physical system with angular frequency $\omega = 2\pi f$. The pressure amplitude of the plane wave radiated from the source is represented in the time domain as a continuous function $s(t)$. In a similar fashion to FMCW radar, the pulse is frequency-swept in a linear fashion between two frequencies f_0 and f_1 (where $f_1 > f_0$) over a time of $\Delta t^* = t_1^* - t_0^*$ (where $t_1^* > t_0^*$). The sound wave changes frequency as $\partial f/\partial t$, radiates toward the snowpack and is reflected at the first interface Ω_1 (Figure 1(a)). The sound wave enters the snowpack and is reflected by the interfaces $\{\Omega_1, \ldots, \Omega_N\}$ that are associated with layers $\{L_1, \ldots, L_N\}$. However, because snow is a dispersive medium, the speed of the pressure wave in the snowpack changes with respect to the frequency of the incident wave. Because the frequency of the source is changing at a rate of $\partial f/\partial t$, the instantaneous phase velocity c_k of the sound pressure wave in a layer L_k of the snowpack will also change in a corresponding fashion below a certain threshold frequency f_t. Using the Biot theory, Albert (1993a) has shown that the phase velocity of the pressure wave in snow will approach the phase velocity of sound in air ($c_k/c_0 \approx 1$) for $f_i \to f_c \approx 10^6$ Hz, where f_i is the instantaneous frequency of the wave. For sound at frequencies less than f_c, we assume that the effective reflection coefficient for each interface $\{\Omega_1, \ldots, \Omega_N\}$ is a function of the frequency-integrated reflection coefficients:

$$\Gamma_k = \frac{1}{f_1 - f_0}\int_{f_0}^{f_1} \Gamma(f_i)\,df_i \tag{14}$$

To determine the average phase velocity of the pulse in the snowpack, it is necessary to consider an analysis by Johnson (1980) and Johnson and Plona (1982) regarding the phase velocity of the slow pressure wave in a porous medium. It is assumed that the compressibility of air in the pore spaces of the snowpack is greater than the compressibility of the skeletal frame of the ice matrix so that the motion of the frame is negligible. Albert (2001) has recognized that this is the case for snow, which is an air-saturated porous material. Thus, as found by Johnson and Plona (1982) and Johnson *et al*. (1982), the average phase velocity of the Biot slow wave in a porous medium is given by:

$$\overline{c}_k = c_0/\sqrt{\alpha_k} \tag{15}$$

Because the acoustic pressure wave travelling in the snowpack is a longitudinal wave, we assume that the reflection of this wave from the layers $\{L_1, \ldots, L_N\}$ will be evident as a longitudinal pressure wave in the air layer L_0 above the snowpack when the reflected wave from an interface Ω_k passes successively through the rest of the layers across the air-snow boundary. It is assumed that the reflected wave from the snowpack consists primarily of longitudinal waves parallel to the $\hat{\mathbf{y}}$-axis of the physical system. The time of the pulse $\Delta t^* = t_1^* - t_0^* \gg t_k$ where t_k is the time required for a pressure wave to traverse a given layer L_k of the snowpack. Thus, the overall reflection $s'(t)$ from the snowpack (Figure 1(a)) will be complicated due to reflections of the continuously-swept wave $s(t)$ from each of the layers. Treating the snowpack as a digital filter with a given response $r(t)$ that is subjected to an attenuation function $a(t)$, the overall reflection $s'(t)$ is:

$$s'(t) = \int_{-\infty}^{+\infty}\int_{-\infty}^{+\infty} s(\tau)r(t-\tau)d\tau a(\tau)d\tau = s(t) * r(t) * a(t) \tag{16}$$

where τ is the intrinsic time shift associated with the convolution process.

MEASURING DEVICE

To be able to capture the overall reflected wave from the snowpack two measuring devices were built. The first consisted of a pair of loudspeakers and a microphone that was mounted on a metal frame (Figure 2). The frame was attached to the end of a 1-m arm that extended over the surface of the snowpack. The arm length was such

DOI: 10.1002/hyp

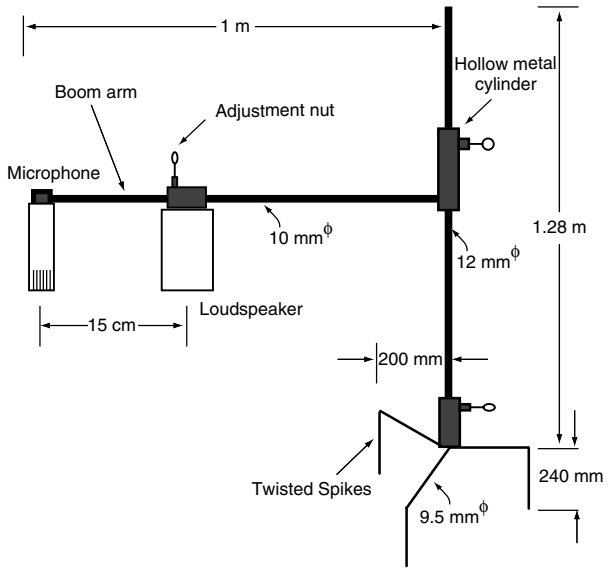

Figure 2. Diagram of metal frame used to hold the loudspeaker and microphone in place over the snowpack for the Saskatchewan sites. The arm length is 1 m, and the distance between the microphone and the speaker could be adjusted, but for all experiments was approximately 15 cm. During deployment, both the speaker and the microphone were situated at distances ranging between 15 and 40 cm above the snow surface. A series of twisted spikes enabled the stand to be pushed into the ground to ensure that the measurement system would be stable

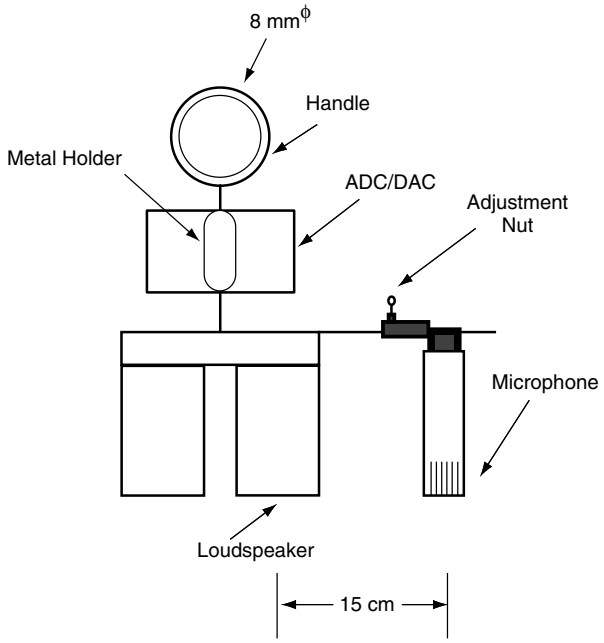

Figure 3. Diagram of the metal frame used to hold the loudspeaker and the microphone in place over the snowpack for the Lake O'Hara sites. The separation distance between the speaker and the microphone was 15 cm. During deployment, both the speaker and the microphone were situated between 15 and 40 cm above the snow surface

that the body of the stand would not interfere with the projected area of the source on the snowpack. The arm could be raised and lowered above the snow surface, but during experiments, the distance of the loudspeaker and microphone above the snow surface ranged between 15 and 40 cm. The separation distance between the speaker and the microphone was approximately 15 cm. The mounting stand of the apparatus was equipped with a set of twisted spikes that enabled the device to be pushed into the ground so that the metal frame holding the loudspeaker and the microphone could be placed perpendicular to the snow surface.

A more portable version was also constructed for carrying the device to a remote field location (Figure 3). This consisted of a smaller metal structure with a shaft and a handle. The same metal frame used on the end of the boom arm was placed on the end of the structure, and the same loudspeaker and microphone were used in all of the trials conducted using both of the stands. The speaker and the microphone were separated by 15 cm. The loudspeaker and the microphone were situated no more than 40 cm above the snow surface.

Owing to its high sensitivity, low noise and wide frequency response (~20 Hz–~20 kHz), the microphone selected for the purpose of this research was a Behringer B-5 gold-sputtered diaphragm condenser microphone. The frequency response of this microphone is generally flat over the frequency range of interest. The B-5 microphone is available with a series of caps that enabled conversion of the microphone's polar pattern to that of a unidirectional cardioid. The microphone had to have a unidirectional configuration in the context of this experiment to attenuate the sound wave that traveled directly from the loudspeaker through the air to the microphone. The residual sound wave from the loudspeaker that was picked up by the microphone was later removed by digital signal processing. Current was supplied to the microphone via an XLR cable connected to a low-noise Rolls +48 V phantom power supply. A 12 V battery pack was used to power this phantom supply via an adapter. Output from the microphone was fed directly into a Behringer FCA202 24-bit analog-to-digital converter (ADC)/digital-to-analog converter (DAC) operating at a sampling rate of $f_c = 96$ kHz. The loudspeaker pair used in this experiment was a battery-powered Koss SXM/7 portable loudspeaker set with an incorporated amplifier. This was attached to the DAC section of the FCA202 interface. Each loudspeaker consisted of a single driver and did not contain crossovers allowing for the use of two transducers (i.e. a middle-range loudspeaker and a tweeter). Thus, although the frequency response of the loudspeaker could not be approximated as flat over the range of the original sweep $s(t)$, additional parallax error would not be caused by the use of two separate drivers. Because both loudspeakers were permanently attached together with a cable, it was impossible to separate them. Consequently, the pulse was produced by only one loudspeaker, and the other loudspeaker was placed next to the first loudspeaker. Both loudspeakers were not driven at the same time to ensure that spatial interference did not occur between the two separate sources.

DIGITAL SIGNAL PROCESSING

As a notational convention, continuous functions in the time domain are shown with curved brackets $(\cdots)$ and

DOI: 10.1002/hyp

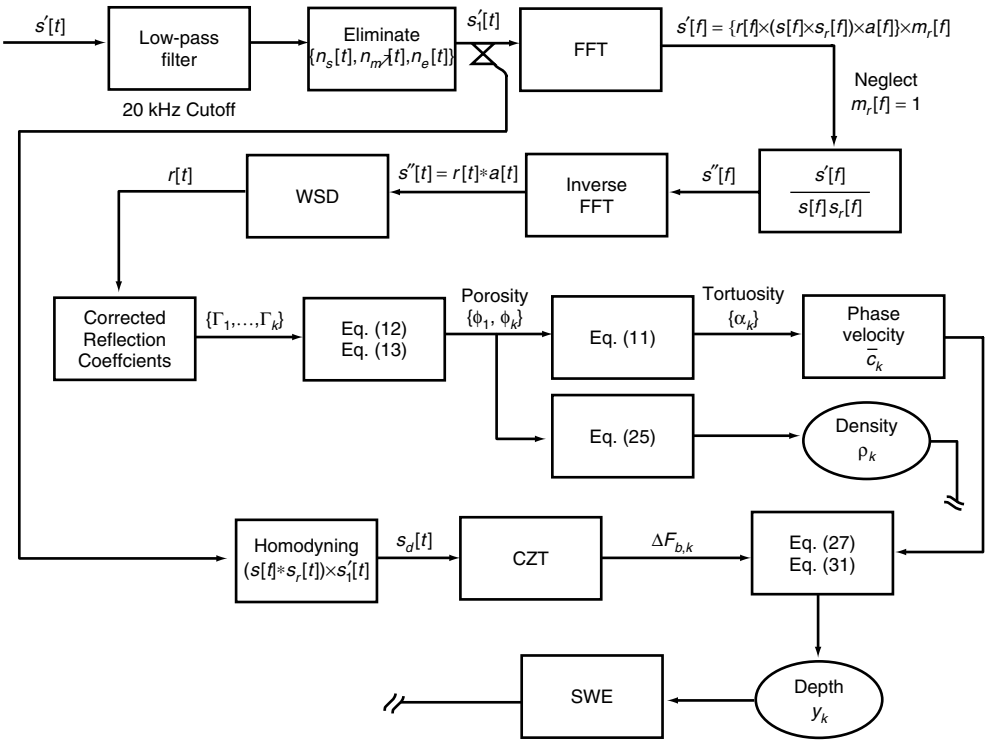

Figure 4. Flowchart of digital signal processing applied in the context of this experiment

discrete signals comprised of an ordered set of numbers by square brackets $[\cdots]$. To include the effects of the measurement system, Equation (16) is rewritten as:

$$s'[t] = \{r[t] * (s[t] * s_r[t]) * a[t]\} * m_r[t] + n_s[t] + n_{m\nearrow}[t] + n_e[t] - (n_s[t] + n_{m\nearrow}[t] + n_e[t]) \quad (17)$$

where $s'[t]$ is the digitally sampled overall reflection response from the snowpack, $r[t]$ is the reflection response consisting of the effective (frequency-integrated) pressure reflection coefficients at each of the interfaces $\{\Omega_1, \ldots, \Omega_N\}$, the original numerically-generated frequency sweep is $s[t]$, the response of the loudspeaker is $s_r[t]$, the attenuation function of the snowpack is $a[t]$, the microphone response is $m_r[t]$, the noise in the recording system and ADC is $n_s[t]$, the sound wave of the original sweep from the loudspeaker that travels directly through the air to the microphone is $n_{m\nearrow}[t]$, and $n_e[t]$ is the noise that is introduced due to environmental phenomena such as wind and blowing snow. If the frequency response of the microphone is flat over the frequency domain of the bandwidth, $m_r[t]$ can be eliminated from Equation (17) since the microphone can be assumed as not playing a significant role in the measurement system.

The offline signal processing followed a flowchart (Figure 4) that ends with the extraction of depth and density data from each of the layers of the snowpack. The first step in the digital processing flow was to low-pass filter the signal $s'[t]$ to ensure that there were no frequency components that were higher than f_1 in the recorded signal. Once $s'[t]$ was filtered, the terms $\{n_s[t], n_{m\nearrow}[t], n_e[t]\}$ were eliminated from the signal by subtraction in the time domain. Each of the signals has the same discrete number of points n_p such that card $(n_s[t], n_{m\nearrow}[t], n_e[t]) = n_p$. Thus, the convolution model (Equation 17) now becomes:

$$s'[t] = \{r[t] * (s[t] * s_r[t]) * a[t]\} * m_r[t] + n_s[t] + n_{m\nearrow}[t] + n_e[t] - (n_s[t] + n_{m\nearrow}[t] + n_e[t]) \quad (18)$$

and

$$s'_1[t] = \{r[t] * (s[t] * s_r[t]) * a[t]\} * m_r[t] \quad (19)$$

The time domain signal $s'_1[t]$ was then taken into the frequency domain by the discrete fast fourier transform (FFT). Because convolution in the time domain is equivalent to multiplication in the frequency domain, Equation (19) becomes:

$$s'[f] = \{r[f] \times (s[f] \times s_r[f]) \times a[f]\} \times m_r[f] \quad (20)$$

It is assumed that the microphone response $m_r[f] = 1$ was flat over the frequency range of interest (so that it does not play a significant role in this equation) and that the frequency response of the loudspeaker $s_r[t]$ has already been determined as $FFT[s[t] * s_r[t]] = s[f]s_r[f]$. Because the frequency response $s[f]$ of the original sweep was known, the reflection response $r[f]$ was expressed as the product:

$$s''[f] = r[f]a[f] = \frac{s'[f]}{s[f]s_r[f]} \quad (21)$$

where $s[f]s_r[f] \neq 0$, so there are no zeros in the frequency spectrum. Division in the frequency domain

DOI: 10.1002/hyp

is used here in lieu of cross-correlation to deconvolve $r[f]a[f]$ from the rest of the signal. Taking $s''[f]$ back into the time domain by the inverse discrete FFT, it follows that:

$$s''[t] = r[t] * a[t] \tag{22}$$

Equation (22) shows that the reflection response $r[t]$ is convolved with the attenuation filter of the snowpack $a[t]$. This expresses mathematically the effects of attenuation on the sound wave that passes through the snowpack. The reflection response $r[t]$ is a signal that is comprised of the reflection coefficient at each interface expressed as a function of time. Thus, local maxima in the time-domain representation of $r[t]$ are the reflection coefficients at each interface. However, the attenuation filter $a[t]$ of the snowpack is unknown. To remove $a[t]$ and to estimate the effective frequency-integrated reflection coefficients at each of the interfaces of the snowpack, the Weiner spiking deconvolution (WSD) method was used to find $r[t]$.

Normally, WSD has been applied in the context of impulse seismology to determine the reflection coefficients at the interfaces of layered rocks. However, in this experiment, WSD was used to extract the reflection coefficients from $s''[t]$. Although Mewhort *et al.* (2002) have argued that spiking deconvolution as applied to a vibroseis dataset (or in this case, a dataset comprised of the overall reflection response) violates the minimum-phase assumption, and according to Gibson and Larner (1984) as well as Brittle and Lines (2001), will therefore cause a phase shift in the data, we applied WSD to only find the reflection coefficients at the interfaces. Because the reflection signal $r[t]$ is in the time domain, the time at which each of the reflections occurs is usually taken to be the time-of-flight to each of the interfaces. Because there might have been a possible phase shift in the data, we do not use the time at which each of the reflections occurs to calculate the distance to the interfaces in the snowpack by the use of kinematics in the same manner as vibroseis signal interpretation. Rather, we implement signal processing particular to FMCW radar to be able to determine the distance to each of the interfaces in the snowpack, thereby using WSD and circumventing the possible violation of the minimum-phase assumption. Nevertheless, Brittle *et al.* (2001) and Brittle and Lines (2001) have implicitly noted that the phase shift in the reflection signal $r[t]$ is caused due to cross-correlation with the reference sweep, an operation that is normally applied in the context of vibroseis signal processing. It is the embedded Klauder wavelet in the cross-correlated dataset that violates the minimum-phase assumption of the deconvolution operation. Thus, Brittle and Lines (2001) support the use of division in the frequency domain before deconvolution is applied because unlike cross-correlation, this does not embed the Klauder wavelet in the resulting $r[t]$ signal, and consequently, it is possible to implement a deconvolution operation on the initial dataset. However some residual phase shifts might occur by the use of deconvolution on a vibroseis dataset. Although WSD attempts to calculate the minimum-phase wavelet, there may be unpredictable behaviour with regard to the phase of the reconstructed reflection response, and it is also for this reason that we do not use the time to each of the reflections to calculate the distances to the interfaces in the snowpack.

WSD (Robinson, 1957) was implemented by adding 0·1% white noise as a stability factor to the time domain dataset $s''[t]$ and then autocorrelating $s''[t]$. The autocorrelation of $s''[t]$ was taken into the frequency domain by the FFT, and spectral factorization calculated the minimum-phase wavelet spectrum. This wavelet spectrum was subjected to the inverse FFT and the inverse wavelet was determined by the use of the Levinson recursion. The inverse wavelet was then convolved with $s''[t]$ by multiplication in the frequency domain to determine the reflection response $r[t]$ consisting of the frequency-integrated pressure reflection coefficients $\{\Gamma_1, \ldots, \Gamma_N\}$ associated with the interfaces $\{\Omega_1, \ldots, \Omega_N\}$ of the snowpack.

If the loudspeaker is too close to the surface of the snowpack such that the surface is not in the far field of the radiated sound source, the extracted reflection coefficients $\{\Gamma_1, \ldots, \Gamma_N\}$ will be spherical, rather than the planar wave pressure reflection coefficients. This might have been the case in these experiments, since the spatial sound fields of the loudspeakers are unknown. To confirm plane wave reflection coefficients, the extracted set $\{\Gamma_1, \ldots, \Gamma_N\}$ was subjected to a numerical correction process described by Harrison and Nielsen (2004) in the context of sonar. Using a Hankel transform of the Sommerfeld integral, the corrected plane wave reflection coefficient for a layer L_k was determined by:

$$\Gamma_{\mathrm{k,corrected}} = \left\{ \frac{\exp\left[j \cdot \left[{k_0}^2 - \left(k_0 \cos\theta_g\right)^2\right] \cdot y_0\right]}{{k_0}^2 - \left(k_0 \cos\theta_g\right)^2} \right\}^{-1} \times j \int_0^{\infty} \Gamma_{\mathrm{k,uncorrected}} \cdot \frac{\exp\left[jk_0\left(r^2 + y_0^2\right)\right]}{\left(r^2 + y_0^2\right)} \times J_0\left[r \cdot k_0 \cos\theta_g\right] r dr \tag{23}$$

where $k_0 = 2\pi f / c_0$ is the angular wavenumber in the air medium, $J_0[\cdots]$ is the Bessel function of the first kind, $\theta_g \to 0$ is the grazing angle of the loudspeaker to the surface of the snowpack, $j = \sqrt{-1}$ represents a complex number and the integration is over r on the interval $[0, \infty)$. Harrison and Nielsen (2004) have shown that this transform is the same even when dealing with a multilayered medium, and does not depend on the medium's geoacoustical parameters. Letting $\theta_g \to 0$ since the loudspeaker was normal to the snow surface, Equation (23) was numerically integrated over $[f_0, f_1]$ so that the reflection coefficients were corrected over the entire frequency range.

Once the corrected reflection coefficients were determined, the porosity of each layer of the snowpack was calculated using Equations (12) and (13). These equations were evaluated using a Newton-Raphson iteration (i.e. Mathews, 1992). The density ρ_1 of the first

DOI: 10.1002/hyp

layer of the snowpack was found by:

$$\rho_1 = \rho_{\text{ice}} \cdot (1 - \phi_1) \tag{24}$$

and this relationship was extended for multiple layers:

$$\rho_k = \rho_{\text{ice}} \cdot (1 - \phi_k) \tag{25}$$

where ρ_{ice} is the nominal density of ice at the freezing point, approximated to be $\rho_{\text{ice}} = 917$ kg m^{-3}.

The tortuosity α_1 was estimated using Berryman's (1980) relationship (Equation 11). Both the porosity ϕ_1 and the density ρ_1 were used recursively along with the reflection coefficients of the successive layers $\{\Gamma_2, \ldots, \Gamma_N\}$ and Equations (12), (13) and (25) to calculate the density of each layer in the snowpack. The tortuosity was used to estimate the phase velocity of the Biot slow wave in each of the layers by the use of Equation (15).

The distance between each of the layers was determined by subjecting signal $s[t]$ and signal $s''[t]$ to a signal processing flow that borrows theory from FMCW radar. First, both $s[t] * s_r[t]$ and $s_1'[t]$, after being low-pass filtered, were mixed together in the time domain by homodyning (point-by-point multiplication, i.e. $(s[t] * s_r[t]) \times s_1[t]$). The resulting signal $s_d[t]$ was then taken into the frequency domain by the Chirp-Z transform (Bluestein, 1968; Rabiner *et al.*, 1969), thereby yielding $s_d[f]$. This particular type of transform is also known as the zoom-FFT because it enables the frequency spectrum to be calculated at a higher resolution for a narrow band of frequencies that can be less than $f_s/2$. The lower frequencies of $s_d[f]$ correspond to the frequency difference between $s[t] * s_r[t]$ and $s''[t]$. Considering each of the interfaces $\{\Omega_1, \ldots, \Omega_N\}$ between the layers of the snowpack to be a reflector, the homodyned wave will contain peaks in the frequency spectrum which correspond to each of the reflectors. The N peaks in $s_d[f]$ are produced due to time delays between each of the reflections at the interfaces between the layers. Figure 5 is a conceptual diagram of the transmitted signal $s(t; f)$ and the reflected time-shifted signals $r_1(t; f), \ldots, r_N(t; f)$ from each of the layers in the snowpack. For reflection from the top of the snowpack, $\Delta F_{b,1} = \Delta f_{b,1}$, and the variables $\{B, \Delta t, \Delta f_1, t_1\}$ were related by the proportionality utilized by Yankielun *et al.* (2004) for FMCW radar:

$$\frac{B}{\Delta t^*} = \frac{\Delta F_{b,1}}{2t_1} \tag{26}$$

By introducing $t_0 = y_0/c_0$, where t_0 is the time taken to travel the one-way distance y_0 from the transducer to the snowpack, and c_0 is the phase velocity of sound in the air layer $k = 0$ above the snowpack, it follows that:

$$y_1 = \frac{\Delta F_{b,1} \Delta t^* \overline{c}_1}{2B} \tag{27}$$

where the average phase velocity $\overline{c}_1$ of the sound wave in the air layer L_0 is calculated with recourse to Raichel (2000), with $\overline{c}_1 = \sqrt{1{\cdot}4RT^*}$, where T^* is the ambient environmental temperature, and R is the thermodynamic gas constant of air.

Alternately, for reflections from a layer L_k of the air-snowpack system with $k > 1$, a modified version of Equation (26) is:

$$\frac{B}{\Delta t^*} = \frac{\left(\Delta F_{b,k} = \sum_{i=1}^{N} \Delta f_{b,i}\right)}{2t_1 + \cdots 2t_k} \tag{28}$$

$$2B\left(\frac{y_1}{\overline{c}_1} + \cdots + \frac{y_k}{\overline{c}_k}\right) = \Delta F_{b,k} \Delta t^* \tag{29}$$

$$\frac{2By_k}{\overline{c}_k} + 2B\left(\frac{y_1}{\overline{c}_1} + \cdots + \frac{y_{k-1}}{\overline{c}_{k-1}}\right) = \Delta F_{b,k} \Delta t^* \tag{30}$$

$$y_k = \frac{\overline{c}_k}{2B}\left(\Delta F_{b,k} \Delta t^* - 2B \sum_{i=1}^{k-1} \frac{y_i}{\overline{c}_i}\right) \tag{31}$$

Equation (31) was used to determine the vertical dimension of each layer $\{L_2, \ldots, L_N\}$. Since the density of each layer was found by Equation (24) and the depth by Equation (31), the SWE of the entire snowpack is:

$$S_E = \varphi \sum_{i=1}^{N} y_k \rho_k \tag{32}$$

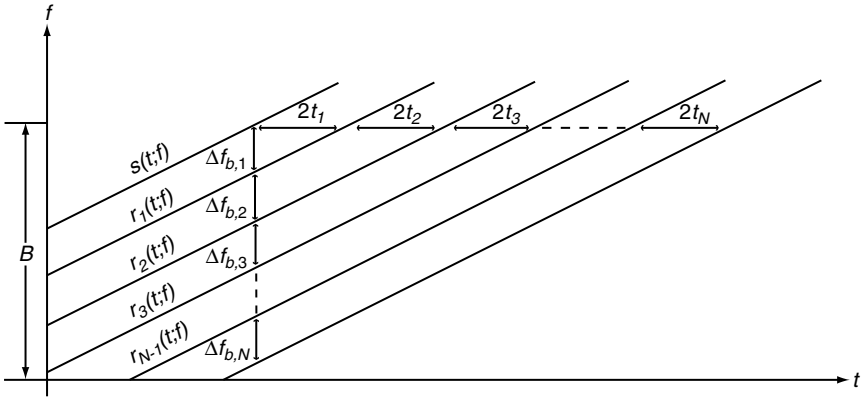

Figure 5. Conceptual diagram of the snowpack response. The signal that is transmitted from the speaker is $s[t, f]$. The reflected signals $r_1[t, f], \ldots, r_N[t, f]$ from each of the layers in the snowpack are shifted in frequency by $\Delta f_{b,k}$ for the *kth* layer of the snowpack system

DOI: 10.1002/hyp

where $\varphi = 1\ \mathrm{m}^2 \cdot \mathrm{kg}^{-2} \cdot \mathrm{mm}$ is a continuity constant, and the implicit assumption is that 1 kg of water has a uniform depth of 1 mm over an area of 1 m^2 (i.e. Pomeroy and Gray, 1995).

EXPERIMENTAL LOCATIONS

The two experimental setups described in this paper were deployed at field sites situated near Saskatoon, Saskatchewan and in Yoho National Park, British Columbia, Canada. Owing to favourable road access, the less portable version of the stand was deployed at the Saskatchewan sites. Because the Lake O'Hara site is only accessible by a 12 km ski or snowshoe journey during the winter months, the portable version of the apparatus was deployed at this location.

The Saskatchewan sites were assigned identifiers which are listed in Table I and are indicative of various Rural Municipalities surrounding Saskatoon (420–540 m above sea level, 52°7′N 106°39′W). The Saskatchewan sites are typical of the agricultural mixed grass prairie region, with gently sloping large fields of grass or grain stubble dotted with aspen stands and shelterbelts along the sides of fields. The British Columbia sites are demarcated by a number in Table II. These sites are typical of sub-alpine forest zone, with evergreen (fir and spruce) stands on slopes up to 15°, interspersed with small grassy clearings. Figure 6 is a photograph indicative of field locations where the method was attempted in Saskatchewan, whereas Figure 7 shows an example photograph of the Lake O'Hara research sites.

Most of the trials of the acoustic sounding method were conducted at the Saskatchewan sites in January and March 2006 and at the Lake O'Hara sites in April 2006. The average temperature at the Saskatchewan sites during the January observations was approximately −8 °C, whilst in March it was above freezing. The January snowpack was observed to be cold and dry, and no appreciable undulations were observed. However, in March active melt was occurring and so the snowpack was very wet because of rapid melt and poor drainage due to impeding ice layers. The maximum cumulative depth of snow observed at the Saskatchewan sites was 0·5 m.

Table I. Overview of Saskatchewan sites. Fetch refers to unobstructed upwind distance for blowing snow transport

Rural municipality and number	Dominant sub-nival vegetation	Average vegetation height (cm)	Forest cover	Slope (°)	Fetch (m)
Dundurn 1	Mixed Grass	10·2	*Aspen Poplar.*	2	<200
Dundurn 2	Mixed Grass	8·7	*Aspen Poplar.*	2	<200
Dundurn 3	Mixed Grass	9·2	Open	2	<600
Bradwell	Mixed Grass	3·9	Open	3	<700
Aberdeen	Mixed Grass	9·9	Open	3	>1000
Corman Park	Mixed Grass	11·5	Open	2	<300
Vanscoy	Mixed Grass	10·6	Open	4	<200

Table II. Overview of Lake O'Hara sites. The identifiers for each site are simply numerical values

Site	Dominant sub-nival vegetation	Average vegetation height (cm)	Forest cover	Slope (°)	Fetch (m)
1	Short grass	10	Fir & Spruce	10	100
2	Short grass	14	Fir & Spruce	15	100
3	Short grass	12	Mixed	15	100
4	Short grass	10	Open	2	300
5	Short grass	10	Mixed	14	100
6	Mosses	0·10	Mixed	2	300
7	Lichen	0·10	Mixed	15	100

Figure 6. Photograph of observation site Dundurn 1 in Blackstrap Provincial Park, Saskatchewan Canada

Figure 7. Photograph showing an example of the Lake O'Hara research sites, British Columbia. The topography of the snow-covered area in the foreground of the photograph is gently undulating, and the forested slopes (with a slope angle of approximately 15°) was also used to collect data

At the Lake O'Hara site, the average air temperature was approximately −3 °C during observations. The snowpack at the Lake O'Hara sites was considerably wetter than the snowpack observed in Saskatchewan during January (but not as wet as that observed in March) because the melt period was beginning. However, the wetness of

DOI: 10.1002/hyp

the snowpack observed at the Lake O'Hara sites was considerably less than the wetness of the snowpack in March 2006 at the Saskatchewan research sites. The maximum cumulative depth of snow observed at the Lake O'Hara site was 1·5 m. Although some minor windflow was present, blowing snow was not observed at either site during observation periods.

PROCEDURE

The mounting stands were taken to each of the sites. Then, the loudspeaker and the microphone were attached to each of the stands, and current was applied to the microphone before it was plugged into the FCA202 interface to ensure that the microphone was stabilized prior to taking measurements. With the first apparatus, a level was used to ensure that the loudspeaker and the microphone were situated perpendicular to the surface of the snowpack. This could not be done for the second, more portable, apparatus due to the lack of a stand. For the second apparatus, the loudspeaker and microphone were held at a position that was believed to be perpendicular to the surface of the snowpack. Then, a frequency-swept sound pulse was sent from the loudspeaker. The duration of the pulse was selected to be $\Delta t^* = 1$ s, but different times of the sweep were also attempted ($\Delta t^* = 0{\cdot}1$ s to 5·0 s). It was found that the $\Delta t^* = 1{\cdot}0$ s sweep gave the best results, and it is these results that are presented in this paper. The bandwidth of the pulse was chosen to be $B = 20000$ Hz $- 20$ Hz $= 19980$ Hz. Although this might have not been the effective bandwidth of the method that was used to characterize the snowpack, these were the frequencies of the reference sweep $s[t]$ that were sent to the loudspeaker. The loudspeaker did not reproduce all frequencies equally, but reproduced a subset of the frequencies that were produced. The sound pressure level (SPL) of the pulse sent into the snowpack was measured with a sound-level meter at the source and was determined to be close to 100 dB at all sites. The ambient environmental temperature T^*, used to determine the phase velocity of the pulse in the first layer L_0 above the surface of the snowpack, was determined by the use of a thermocouple.

After the acoustic measurement had been taken, the depth and density of the snow was determined by a ruler and gravimetric sampling. The sampling point for this measurement was situated directly underneath of the loudspeaker. At locations where the layers of the snowpack were visible, gravimetric samples were taken from each of the layers. Gravimetric sampling was the primary means of determining physical measurements at each of the Saskatchewan sites. Gravimetric snow sampling using a snowpit could not be conducted at the Lake O'Hara site and a snow tube was used to estimate density.

The three signals $\{n_s[t], n_{m\nearrow}[t], n_e[t]\}$ were determined immediately prior to experimentation and field work. The noise in the system was determined by the use of a loopback test, where a cable was used to connect the input of the ADC to the output of the DAC. Then, a $\Delta t = 1$ s sample was taken with the cables attached. This was thought to be representative of the noise in the system. The sound wave of the original sweep from the loudspeaker that travels directly through the air to the microphone $n_{m\nearrow}[t]$ was determined by taking a $\Delta t = 1$ s sample with the microphone situated under the loudspeaker, but at a 90° angle to the driver so that the sound would arrive directly on the side of the microphone. Because the loudspeaker and the microphone were situated parallel to each other, this measurement of $n_{m\nearrow}[t]$ was believed to be indicative of the oblique wave from the loudspeaker that traveled through the air and was consequently received from the microphone. The noise $n_e[t]$ caused by environmental phenomena such as wind was found by taking successive $\Delta t = 1$ s samples for 5 min at each of the field locations. One sample was taken every 10 s. This procedure was followed to ensure that an adequate representation of the environmental noise at the field site could be determined. This included additional noise caused by wind gusts. The samples were then averaged together to find the overall average environmental noise $n_e[t]$.

The signal sent out from the loudspeaker $s[t] * s_r[t]$ was determined by placing the microphone close to the loudspeaker and recording the frequency-swept wave at a 0° (direct-on) angle of incidence for a time of $\Delta t = 1$ s. Although the presence of the microphone might have affected the spatial sound field of the loudspeaker, this provided a crude estimate of the sound wave $s(t)$ that was sent into the snowpack. Further attempts in deploying this apparatus might rely on the use of mathematical modelling to reconstruct the sound wave $s[t] * s_r[t]$ sent from the loudspeaker, given that the frequency response $s_r[t]$ of the loudspeaker can be determined.

RESULTS

The results of this method are considered in the two following sections. In the first section, the application of this method is demonstrated for two different layered snowpacks. In the second section, the data pertaining to SWE is considered.

Snowpack with N = 1 layers

The signal processing flow (Figure 4) was applied to a one-layered snowpack that was observed at the DRM1 site. Time domain representation of the signals being used in this analysis is given in Figure 8. The original wave sent from the speaker into the snowpack is given as Figure 8(a), whereas Figure 8(b) is the raw (unprocessed) signal received at the microphone. By spectral division in the frequency domain, the signal $s'[t] * a[t]$ is determined. The spectral division was observed to be stable, so there were no zeros in the frequency domain. After subjecting the signal to Weiner deconvolution, the

DOI: 10.1002/hyp

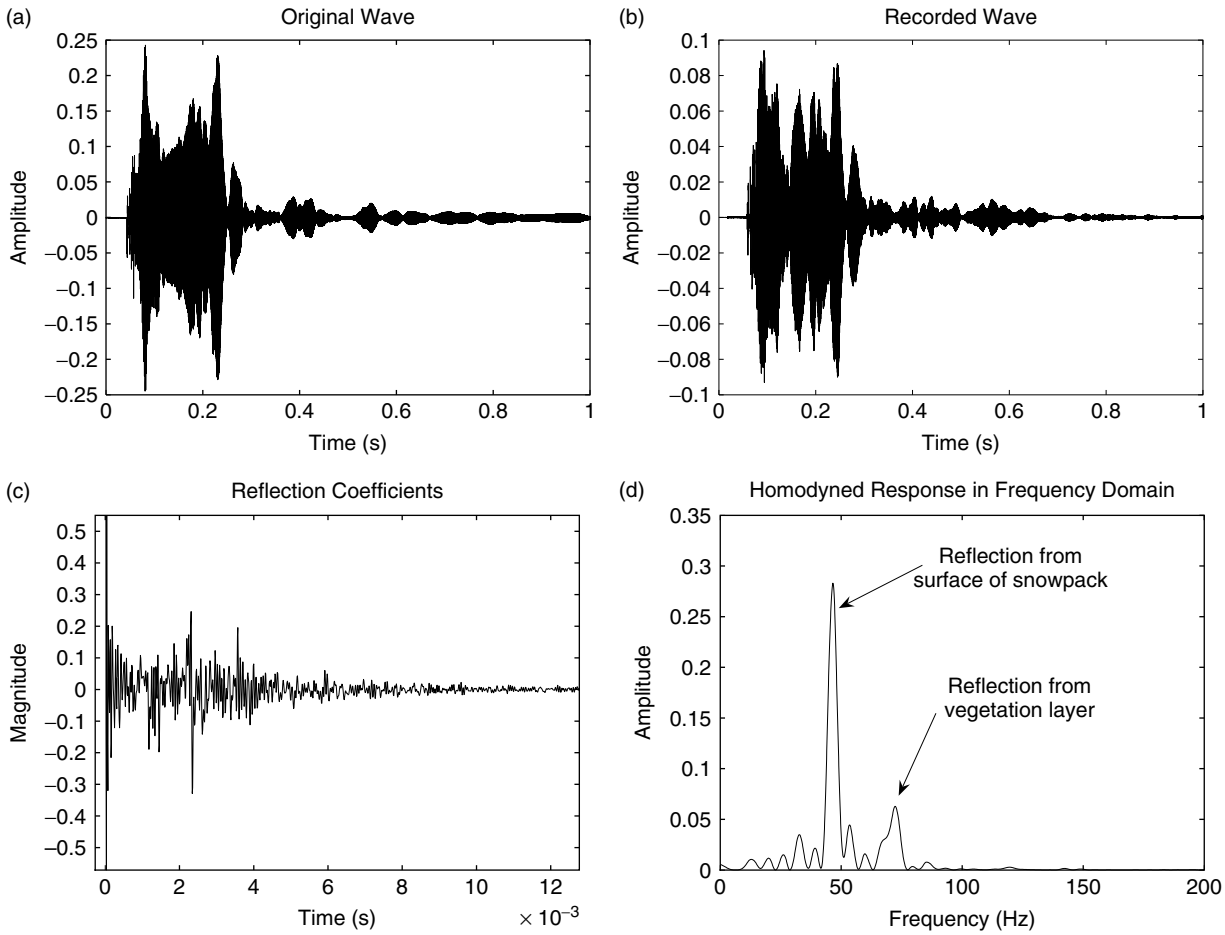

Figure 8. Signals in the time and frequency domains for the $N = 1$ layered snowpack. (a) original wave, (b) recorded wave, (c) reflection coefficients, (d) homodyned response in frequency domain. The amplitudes of Figure 8(a), (b), and (d) are normalized. The beat frequency $\Delta F_{b,k}$ is given in Figure 8(d)

reflection coefficients at each of the interfaces are represented in the time domain (Figure 8(c)). The large spike at the beginning of the signal is assumed to be caused by the starting circuitry associated with the ADC. There were no observed zeros in the frequency domain. Because there is only one such reflection (as marked on Figure 8(d)), it is apparent that this is from the surface of the snowpack. By inspection of Figure 8(c), it appears that $\Gamma_1 = 0{\cdot}22$. The corrected reflection coefficient, calculated using Equation (23), is $\Gamma_1 = 0{\cdot}20$. This is taken to be the plane wave reflection coefficient at the interface Ω_1 of the snowpack. By Newton-Raphson iteration of Equation (12), the porosity of the first layer of the snowpack was found to be $\phi_1 = 0{\cdot}75$. Applying Equation (24), the density of the snow was determined from the porosity as 229 kg m^{-3}. Because only one layer of snow was clearly visible, gravimetric sampling using a scoop could be performed. For comparison, the density determined by gravimetric sampling was 233 kg m^{-3}. The percentage difference between the density determined by the acoustic method and the density determined by gravimetric sampling is approximately 2%.

Assuming that at the Saskatchewan sites, snow can be considered to have a geometry such that $\gamma = 0{\cdot}80$, the tortuosity of the first layer of the snowpack was found to be $\alpha_1 = 1{\cdot}25$. The reason for this choice of γ is discussed in the sensitivity analysis section of this paper. Although there are no widely-published values for the tortuosity of snow, Jones *et al.* (1999) mention that this quantity has been assumed to be approximately equal to unity ($\alpha \approx 1$). The value that we have found for the tortuosity of the snow ($\alpha_1 = 1{\cdot}25$) seems to be in general agreement with this observation. However, we caution that further research is necessary to verify this claim.

By use of Equation (15), the average phase velocity of the Biot slow wave was calculated as $\overline{c}_1 = 296$ m s^{-1}. This is in the range of Albert's (1993a) calculated values for the Biot slow pressure wave in snow, and it is less than the speed of sound in the air layer above the snowpack. This helps to support the notion that we are dealing with the Biot slow wave. To determine the depth of snow, the signal $s''[t]$ is homodyned with the original signal that has been sent out from the speaker. After taking the Chirp-Z transform of the homodyned signal, the frequency spectrum indicates that there are two peaks indicative of reflections thought to be from the top of the snowpack and from the vegetation at the bottom of the deposited snow layer (Figure 8(d)). The first peak is found at a beat frequency of $\Delta F_{b,1} = 46{\cdot}6$ Hz. The phase velocity of the sound wave in the air layer above

DOI: 10.1002/hyp

the snowpack was calculated to be 330 m s^{-1} at a temperature of $-2{\cdot}2\,^{\circ}C$. By the use of Equation (27), the distance to the top of the snowpack from the speaker and microphone was determined to be 0·38 m. Alternately, the distance from the speaker to the top of the snowpack was measured to be 0·35 m. The percentage difference between the two measurements is approximately 9%. Then, recursively applying Equation (31) for the second frequency peak at $\Delta F_{b,2} = 72{\cdot}3$ Hz, the depth of the one-layered snowpack was found as $y_1 = 0{\cdot}19$ m. This initially appeared to differ from the measured depth of snow, which was determined to be 0·28 m, and it was thought to represent an approximate 36% error between the measurement of snow depth by the use of the acoustic method and the measurement of snow depth by the use of a rod. However, this discrepancy between actual and measured depths may be explained by considering that the measured snow depth is the depth to the unvegetated ground surface. Because the depth of vegetation was measured to be 0·08 m, subtraction of this depth from the measured depth to the ground surface yields 0·20 m. This revised estimate of the snow depth represents a 5% difference between the measured and acoustically-determined depth of snow on the ground surface. This simple test case may suggest that scattering and attenuation of the sound wave by vegetation will only permit physical parameters of the snowpack to be determined to the top of the vegetation layer. However, further research is required to assess the effects of vegetation on this method. This includes considering whether the vegetation density structure or objects (such as buried twigs or leaves) contained in the snowpack will affect this method.

Finally, calculating the SWE of the snow layer using the depth and density of snow determined by the acoustic data, it was found by the use of Equation (32) that the SWE was $S_{E,a} = 43{\cdot}5$ mm. Alternately, using gravimetric data, the SWE was calculated as $S_{E,m} = 46{\cdot}6$ mm. This represents a difference of calculated SWE of approximately 7% between both of the methods. By repeating this calculation without using the correction of Equation (23) and taking the reflection coefficient to be $\Gamma_1 = 0{\cdot}22$, the acoustically-determined SWE was determined to be $S_{E,a} = 53{\cdot}2$ mm. This represents a difference of approximately 14% between both of the methods. By correcting the reflection coefficient for potential spherical spreading, it is apparent that the percentage difference between the methods is reduced by 7%.

Snowpack with multiple layers

The same procedure for the $N = 1$ case was repeated for a snowpack containing multiple layers. As shown by this example, these layers do not usually correspond with the layers of a snowpit. This is characteristic of most observations at the Saskatchewan and Lake O'Hara sites. The numerical results of this calculation are summarized in Figure 9 and Table III. The shape factor $\gamma \simeq 0{\cdot}70 > 1/2$ was utilized for the calculation of this example. The snowpack was observed at the Lake O'Hara site, and the phase velocity of the sound wave in the snowpack gradually decreased with depth. By the use of Equation (32), the acoustically-determined SWE was determined to be $S_{E,a} = 288$ mm. The SWE determined by gravimetric sampling was determined to be $S_{E,m} = 297$ mm. This represents an approximate 3% difference between the SWE values determined by the two techniques. When the same method is attempted without using the correction of Equation (23), the SWE is calculated to be $S_{E,a} = 320$ mm. This represents a difference of approximately 8% between both of the methods. Thus, although information from the snowpack may be obtained by the 'inverse problem', this case may demonstrate that the method also works for snowpacks in which discrete layers cannot be readily observed.

Table III. Calculations for a layered snowpack exhibiting a gradual increase of density with depth. The distance from the loudspeaker and the microphone to the first interface of the snowpack is $y_0 = 0{\cdot}18$ m. The surface of the snowpack is coincident with a beat frequency of $\Delta F_{b,1} = 22$ Hz. The depth y_{k-1} is the calculated depth of the layer L_{k-1}. Thus, y_{k-1} is the distance between interfaces Ω_{k-1} and Ω_k. The last interface Ω_{14} has been neglected because this is presumed to be the frozen ground and is not of interest in calculating SWE. The distance $y_{13} = 0{\cdot}32$ m is the vertical dimension of layer L_{13}. Values in this table represent rounded estimates

Interface number (k)	$\Delta F_{b,k}$ (Hz)	Γ_k	ϕ	ρ_k(kg m^{-1})	α_k	$\bar{c}_k$(m s^{-1})	y_{k-1} (m)
1	22	0.16	0.79	211	1.19	304	0·18
2	35	0.01	0.78	222	1.20	302	0·099
3	41	0.017	0.76	241	1.22	299	0·045
4	48	0.011	0.75	253	1.24	298	0·052
5	53·5	0.015	0.73	269	1.26	295	0·041
6	59·5	0.021	0.71	291	1.29	292	0·044
7	66·5	0.01	0.70	301	1.30	290	0·051
8	72·5	0.011	0.69	312	1.32	288	0·044
9	79·4	0.013	0.67	325	1.34	286	0·050
10	87	0.013	0.66	338	1.36	284	0·054
11	91	0.011	0.65	348	1.37	282	0·028
12	97	0.011	0.64	358	1.39	281	0·042
13	104	0.012	0.63	369	1.41	279	0·049
14	150	N/A	N/A	N/A	N/A	N/A	0·32

DOI: 10.1002/hyp

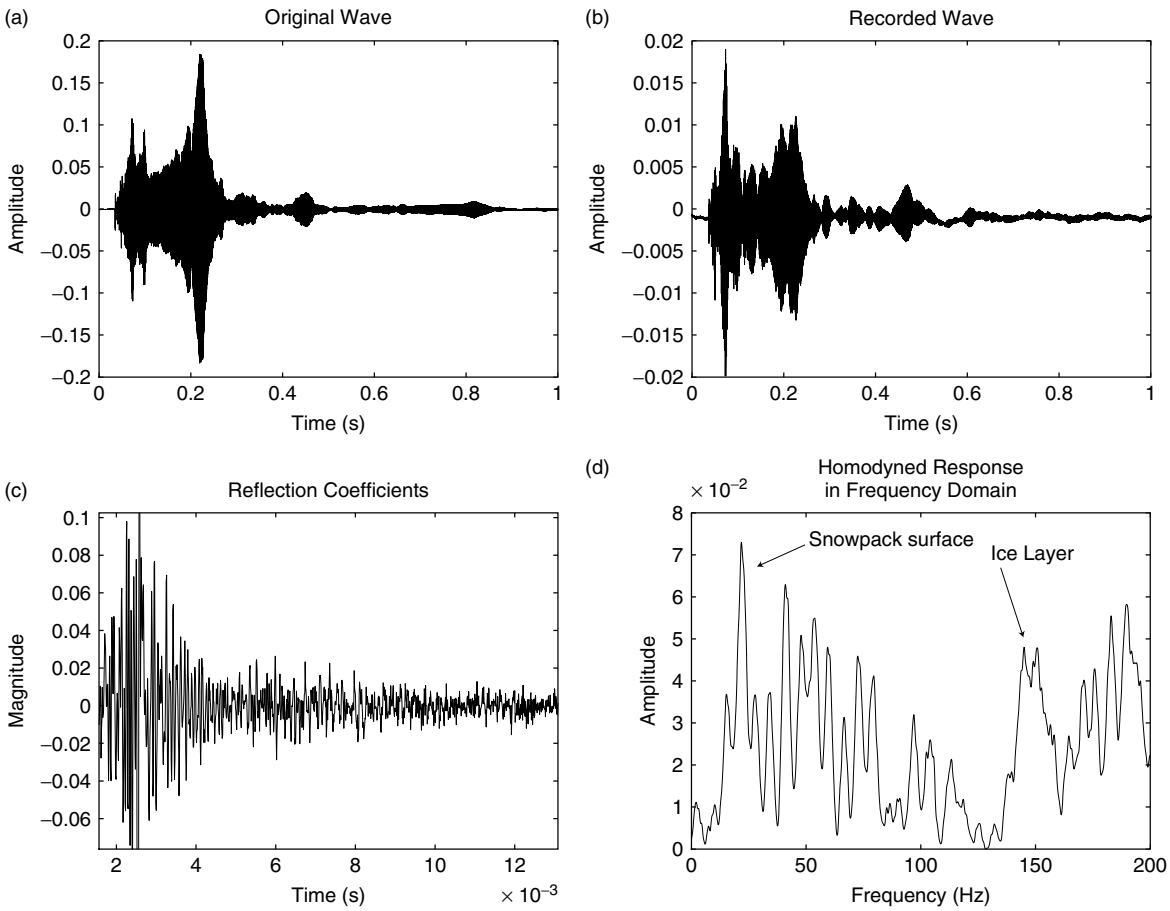

Figure 9. Example for the snowpack with many layers not easily distinguishable. (a) original wave, (b) recorded wave, (c) reflection coefficients, (d) homodyned response in frequency domain. It is believed that the reflections after the beat frequency of 150 Hz are from a frozen layer of ice near the ground. The amplitudes of Figure 8(a), (b), and (d) are normalized. The beat frequency $\Delta F_{b,k}$ is given in Figure 9(d)

Overview of SWE data

For the Saskatchewan observations, the correlation between the measured and the modeled SWE (Figure 10) for dry snow (January) was $r^2 = 0{\cdot}86$ (slope $= 1{\cdot}12$; Root Mean-Squared Error $= 9{\cdot}7$ mm) from 84 samples. These samples were collected from sites that all had vegetation (grass and shrub) heights <30 cm, no visible ice layers, and smooth interfaces between the snow layers. For wet snowpacks (March), the calculated results from 35 samples showed a very weak correlation of $r^2 = 0{\cdot}30$ (slope $= 0{\cdot}51$, root mean-squared error $= 92{\cdot}7$ mm) between the measured and the modeled values of SWE. This was interpreted as being caused by excessive attenuation of the acoustic pressure wave due to the liquid water filling the pore spaces of the snow-ice matrix.

At Lake O'Hara, the majority of physical density samples were collected by the use of an older MSC snow sampling tube. Snow was melting slowly and so a mixture of dry snow and moderately wet, well drained snow was sampled. For all of these sites, the correlation between the values of measured and modeled values of SWE (Figure 11) was found to be $r^2 = 0{\cdot}78$ (slope $= 1{\cdot}02$; root mean-squared error $= 7{\cdot}0$ mm) from 84 samples.

The root mean-squared error is slightly higher for the Saskatchewan sites due to greater variance in the data. This is because the acoustic estimates at

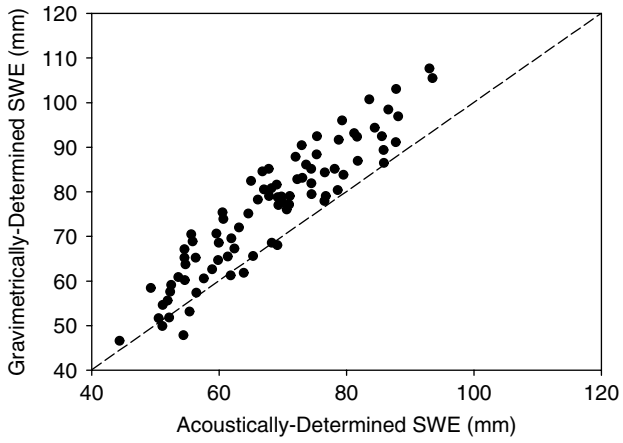

Figure 10. Saskatchewan site results for the relationship between gravimetrically measured and acoustically-determined SWE for January, dry snow conditions. The dashed pattern represents the 1 : 1 line

the Saskatchewan sites were performed over a larger geographic area and range of snowpack type than the estimates performed at the Lake O'Hara sites. It was suspected that the correlation for the Lake O'Hara sites showed a weaker relationship as compared to the correlations found from the Saskatchewan sites due to (1) higher snow liquid water content than the dry prairie snow sites in January, and (2) the presence of a more layers in

DOI: 10.1002/hyp

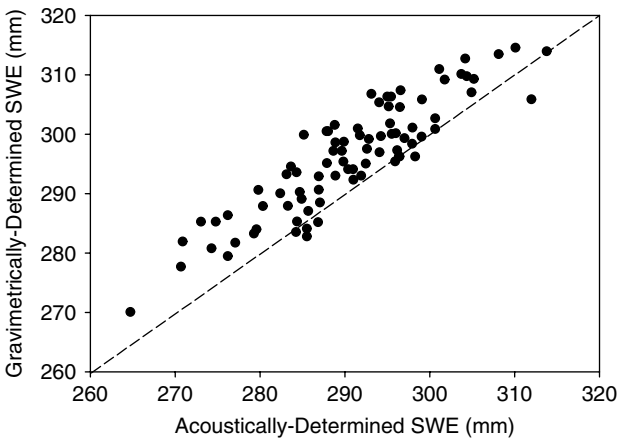

Figure 11. Lake O'Hara site results for the relationship between gravimetrically-measured and acoustically-determined SWE. The dashed pattern represents the 1 : 1 line

the snowpack. The maximum depth of snow tested at the Lake O'Hara sites was 1·5 m, thereby indicating the method's utility for deep mountain snowpacks as well as shallow prairie snowpacks.

Both Figures 10 and 11 indicate that there is a systematic shift in the data, with the gravimetrically-determined SWE being greater than the acoustically-determined SWE estimates. It is conceivable that this shift might have occurred due to depth measurements made from the reflections from each of the interfaces in the snowpack. Because the phase velocity of the sound wave in the snowpack varies with frequency, the acoustically-determined depth of snow is less than the depth of snow determined by physical measurement. This is because the sound wave will travel at different phase velocities in the snowpack at different frequencies. Thus, because the depth of snow is underestimated by the acoustic measurement, the gravimetrically-determined SWE is greater then the acoustically-determined SWE. However, further research is required to verify this claim.

SENSITIVITY ANALYSIS

A sensitivity analysis was performed to determine the effect of the most uncertain parameters on the calculations. The most uncertain parameter is the γ shape factor, which is used in Equations (12) and (13) to determine the porosity of each layer and the tortuosity. Because the porosity is used to calculate both the density and the average phase velocity in each layer, the sensitivity of the γ shape factor is crucial to calculated SWE. Two cases are considered: (1) the sensitivity of γ at the air-snow interface; and (2) the sensitivity of γ at snow-snow interfaces.

Figure 12 shows the results of a sensitivity analysis where γ was varied on the interval (0·5 1·0), which represents the range of the particle shape factor γ and a range

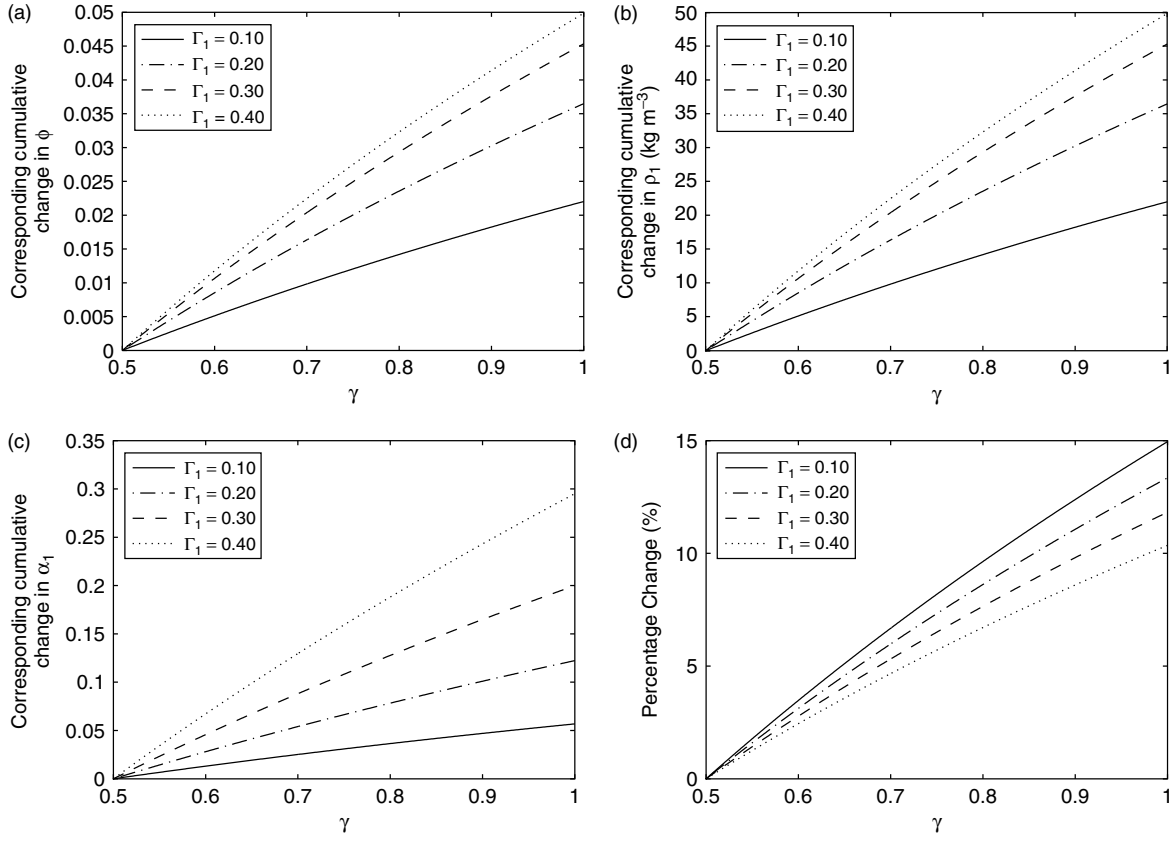

Figure 12. Sensitivity analysis for the air-snow interface. (a) Examining sensitivity of ϕ to change in shape factor γ; (b) Examining sensitivity of ρ_1 to change in shape factor γ; (c) Examining sensitivity of α_1 to change in shape factor γ; (d) Percentage difference of ρ_1 due to change in shape factor γ

DOI: 10.1002/hyp

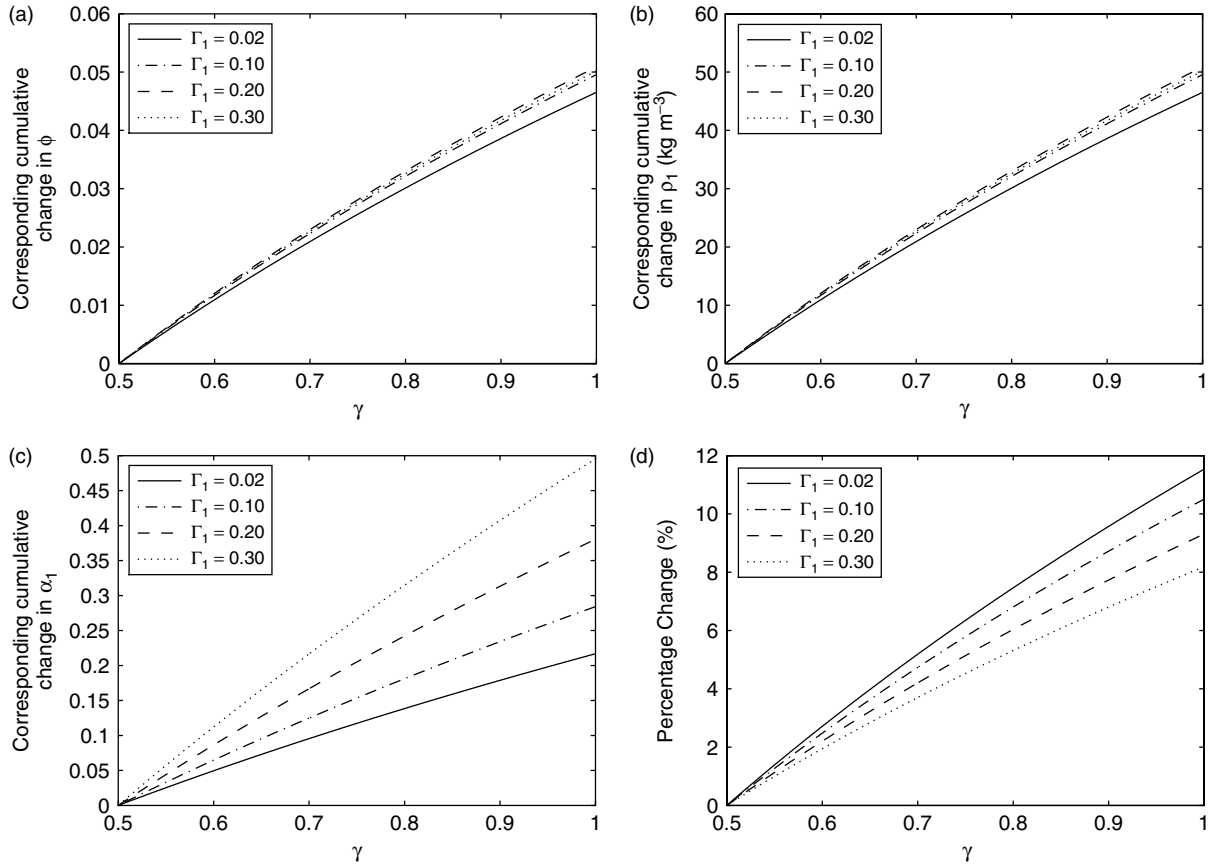

Figure 13. Sensitivity analysis of the snow-snow interface. (a) Examining sensitivity of ϕ to change in shape factor γ; (b) Examining sensitivity of ρ_1 to change in shape factor γ; (c) Examining sensitivity of α_1 to change in shape factor γ; (d) Percentage difference of ρ_1 due to change in shape factor γ

of reflection coefficients, Γ_1. The results indicate that for larger reflection coefficients at the air-snow interface, the cumulative changes in the calculated porosity ϕ_1, density of the first layer ρ_1, and tortuosity α_1 are greater than for the changes observed with reflection coefficients of a lower magnitude. Moreover, for reflection coefficients of a greater magnitude, the cumulative change in the calculated density will be of a corresponding greater magnitude. The numerical experiments show that if the shape factor is selected from the interval (0·5 1·0), the error in the determined density ρ_1 will be no greater than approximately 15%. This indicates that the calculated density ρ_1 is relatively insensitive to variations in γ. Figure 13 indicates a similar trend for the snow-snow interfaces in the snowpack; however, the corresponding change in the calculated porosity ϕ_k and density ρ_k are less sensitive to variations of the reflection coefficient. However, the calculated tortuosity α_k exhibits approximately the same sensitivity as shown in Figure 13. The percentage change in the calculated density due to variations in the γ shape factor at the snow-snow interfaces is approximately the same as the change in the variation in the γ shape factor at the air-snow interface. Using the aggregated data for this experiment, it was found that $\gamma \simeq 0{\cdot}80 > 3/4$ for the Saskatchewan sites best fitted the acoustic estimation of SWE to gravimetric samples, whereas for the Lake O'Hara sites, $\gamma \simeq 0{\cdot}70 > 1/2$ resulted in the best fit. Owing to melt metamorphism, it is conceivable that the snow crystals at the Lake O'Hara site would have more of a spherical shape than the snow crystals at the Saskatchewan site. However, because observations were not made of the snow crystal geometry at both of the sites, it is not possible to make quantitative comparisons and the differences in γ could be due to other factors.

Another uncertainty is introduced by the use of Equation (23), which may correct for some spherical spreading of the sound wave. Applied to the data for the Saskatchewan sites, Equation (23) reduces the percentage error between the acoustically-determined and gravimetrically measured calculations by approximately 5%. Applying Equation (23) to the data for the Lake O'Hara sites, the percentage error is reduced by approximately 8%. This may indicate that Equation (23) has the potential to introduce some minor corrections into the calculations for SWE.

DISCUSSION AND CONCLUSIONS

This paper suggests that sound can be used to determine the physical properties of snow and has presented a theory that allows for the calculation of SWE by the use of an acoustic wave. This helps to support the notion that a simplified version of the Biot theory can be used to determine the physical properties of seasonal snowcovers.

DOI: 10.1002/hyp

Although snow is a porous, lossy medium, it has been suggested that it is possible to determine the physical properties of a snowpack at depths up to 1·5 m. This represents the greatest depth of snow that has been observed in the context of this study. Further research is planned to verify this conclusion.

The Biot slow wave that propagates in the air spaces of the snowpack was used to determine SWE. This method relies on the reflection of sound from the 'layers' in a snowpack that have been created by metamorphism, melt, sublimation, blowing snow and depositional processes. The method does not take into consideration changes in physical properties that increase with depth within a layer because it depends on reflections that are caused by changes in acoustic impedance. However, the example of a snowpack with multiple layers showed that an almost linear decrease in the speed of sound occurs with increasing depth below the surface of the snowpack. This indicates that although it may be possible to determine the physical properties of the snowpack by the use of the overall reflection, the presence of a velocity gradient is apparent by examining discrete samples with regard to depth. By curve fitting, it may be possible to approximate the velocity gradient with depth and then use this approximation to improve estimates of SWE.

Another aspect of acoustic measurement of snow that would benefit from further research is a study of the effects of irregular snow-surface topography and vegetation on the reflection response of the signal. It is possible that in the same manner as any other diffuse reflector, vegetation will cause scattering of the reflected sound wave, thereby decreasing the effectiveness of the method. It is also conceivable that a similar effect could occur when the snow surface is irregular. There is also a possibility that the depth can only be determined to the top vegetation layer. In a similar fashion, one of the tests presented by Albert (2001) showed that the acoustic waveform inversion may occasionally determine only the depth to a particular interface in the snowpack. Other effects of scattering may be caused by ice layers in the snowpack. We did not find these effects in our field trials but they may impact the general applicability of the technique.

Noting these concerns, the overall error in the gravimetrically measured SWE and the SWE determined by the acoustic technique at all of the sites for dry to moderately wet snow conditions was approximately 10%. An analysis given by Goodison *et al.* (1981) indicates that the mean maximum error between SWE determined by a gravimetric snow sampler and SWE determined by carefully weighing bagged samples is approximately 10%. This suggests that the acoustic technique has an average error that is similar to the use of a gravimetric snow sampler. The estimates of SWE presented here are therefore likely adequate for use in snow surveying for hydrological and climatological purposes and are certainly as good as two gravimetric methods compared to each other. Further physical refinement of the device and calibration of its output would reduce these errors.

Further experimentation is planned to both verify the results reported in this paper and extend the method so that it is sufficiently reliable and robust for operational use. One task of additional research would be to determine the effective frequency range over which the sweep can be used to characterize snow. Additional research would help to verify the relationships identified in this paper and further investigate the limitations of the method in the context of other environmental situations.

ACKNOWLEDGEMENTS

Support from an NSERC Discovery Grant, the Canada Research Chairs Programmes (JWP) and a NSERC PGS-M Scholarship (NJK) are gratefully acknowledged. Special thanks to Dr. Masaki Hayashi and Jaime Hood, University of Calgary, Warren Helgason, University of Saskatchewan and to Yoho National Park for assisting us in using the Lake O'Hara site. We thank two anonymous reviewers, whose comments have greatly improved this paper.

SYMBOLS

S_E	Snow water equivalent (kg m^{-2} or mm)
$\{L_1, \ldots, L_N\}$	Snowpack layer identifiers (i.e. Figure 1(a))
L_0	Air layer above the surface of the snowpack
$\{\Omega_1, \ldots, \Omega_N\}$	Interfaces between the layers of the snowpack (i.e. Figure 1(a))
$\overline{c}_k$	The average phase velocity of the slow wave in layer L_k (m s^{-1})
ξ_k	The acoustic impedance of a layer L_k(kg m^{-2} s^{-1})
ω	Angular frequency of air pressure wave at source (rad s^{-1})
f	Frequency of air pressure wave at source (Hz or s^{-1})
y_0	Distance from the source to the surface of the snowpack (m)
y_k	Vertical dimension of layer L_k (m)
Y_N	Total depth of snow in the snowpack (m)
p_0^+	Pressure of the air wave approaching the snowpack surface (Pa)
p_0^-	Pressure of the reflected wave from the snowpack surface (Pa)
p_1^t	Pressure of the wave transmitted into the snowpack (Pa)
c_0^+	Phase velocity of the air wave approaching the snowpack surface (m s^{-1})
c_0^-	Phase velocity of the reflected wave from the snowpack surface (m s^{-1})

DOI: 10.1002/hyp

Γ_k	Pressure reflection coefficient at snowpack interface Ω_k (dimensionless)
$\alpha(\omega)$	Frequency-dependent dynamic tortuosity (dimensionless)
γ	Shape factor dependent on the particle geometry of the porous medium
ϕ_k	Average porosity of a layer L_k of the snowpack
$s(t)$	Pressure amplitude of the plane wave at the source (Pa)
f_0	Starting frequency of the linear frequency sweep (Hz)
f_1	Ending frequency of the linear frequency sweep (Hz)
$B = f_1 - f_0$	Bandwidth of the linear sweep (Hz)
t_0^*	Starting time of the linear frequency sweep (s)
t_1^*	Ending time of the linear frequency sweep (s)
Δt^*	Total time (s) of the frequency sweep
$\partial f/\partial t$	Rate of change of linear sweep (Hz s^{-1})
c_k	Instantaneous phase velocity of sound pressure wave in layer L_k (m s^{-1})
f_i	Instantaneous frequency of the sound pressure wave (Hz)
f_c	Critical frequency of the sound pressure wave (Hz)
f_t	Threshold frequency (Hz)
$\overline{c}_k$	Average phase velocity of the sound pressure wave in layer L_k (m s^{-1})
t_k	The one-way time (s) required for a pressure wave to traverse a given layer L_k
$T_k = 2t_k$	Total round-trip time (s) taken to traverse a given layer L_k of the snowpack
$s'(t)$	Overall reflection from the snowpack (as a continuous function)
$s'[t]$	Overall reflection from the snowpack (as a discrete function)
$r(t)$	Reflection response of the snowpack (as a continuous function)
$r[t]$	Reflection response of the snowpack (as a discrete function)
$a(t)$	Attenuation function of snow as a porous (lossy) medium
$a[t]$	Attenuation function of snow (discrete function)
τ	Time shift caused by the convolution process (s)
λ_0	Wavelength of sound pressure wave in air (m)
f_s	Sampling frequency of the Analog-to-Digital Converter (Hz)
$s[t]$	Original digitally-generated frequency sweep
$s_r[t]$	Frequency response of the loudspeaker in the time domain
$m_r[t]$	Frequency response of the microphone in the time domain
$n_s[t]$	Noise introduced by the recording system
$n_{m\nearrow}[t]$	Sound wave of the original sweep from the loudspeaker that travels directly through the air to the microphone
$n_e[t]$	Noise introduced due to wind and blowing snow
n_p	Number of samples of each of the signals collected
$card(\cdots)$	The cardinality, which is the number of elements in the set $(\cdots)$
$s''[t]$	Convolution of the reflection response of the snowpack with its attenuation
k_0	Angular wavenumber in the air medium (m^{-1})
$FFT[\cdots]$	Denotes application of the discrete FFT to $[\cdots]$
ρ_{ice}	Approximate density of ice (917 kg m^{-3})
$\overline{\rho}_k$	Average bulk density of a layer L_k(kg m^{-3})
$s_d[f]$	Homodyned signal as a result of the signal processing flow
N	Total number of layers in the snowpack
t_0	Time taken for the sound to travel to the snow surface (s)
T^*	Ambient environmental temperature (Kelvin)
$\Delta f_{b,k}$	Frequency shift caused by reflection from interface Ω_k (Hz)
$\Delta F_{b,k}$	Total frequency shift caused by reflection from interface Ω_k (Hz)
$\varphi = 1\ \text{m}^2\cdot\text{kg}^{-2}\cdot\text{mm}$	Continuity constant for calculation of SWE
$R = 287\ \text{N}\cdot\text{m}\cdot\text{kg}^{-1}\cdot\text{K}^{-1}$	Thermodynamic gas constant for air
ρ_0	Equilibrium air density (kg m^{-3})
$J_0[\cdots]$	Bessel function of the first kind
θ_g	Grazing angle of incidence (rad)
$j = \sqrt{-1}$	Complex number

REFERENCES

Albert DG. 1987. The effect of snow on vehicle-generated seismic signatures. *The Journal of the Acoustical Society of America* **81**(4): 881–887.

Albert DG. 1993a. *Attenuation of outdoor sound propagation levels by a snow cover*. CRREL Report 93-20, Cold Regions Research and Engineering Laboratory, Hanover, NH, 1–104.

Albert DG. 1993b. A comparison between wave propagation in water-saturated and air-saturated porous materials. *Journal of Applied Physics* **73**(1): 28–36.

Albert DG. 2001. Acoustic waveform inversion with application to seasonal snow covers. *The Journal of the Acoustical Society of America* **109**(1): 91–101.

Albert DG, Orcutt JA. 1989. Observations of low-frequency acoustic-to-seismic coupling in the summer and winter. *The Journal of the Acoustical Society of America* **86**(1): 352–359.

Albert DG, Orcutt JA. 1990. Acoustic pulse propagation above grassland and snow: comparison of theoretical and experimental waveforms. *The Journal of the Acoustical Society of America* **67**(1): 93–100.

Attenborough K, Buser O. 1988. On the application of rigid-porous models to impedance data for snow. *Journal of Sound and Vibration* **124**(2): 315–327.

Berryman JG. 1980. Confirmation of Biot's theory. *Applied Physics Letters* **37**(4): 382–384.

Berryman JG. 1983. Effective conductivity by fluid analogy for a porous insulator filled with a conductor. *Physical Review B* **27**(12): 7789–7792.

Biot MA. 1956a. Theory of propagation of elastic waves in a fluid-saturated porous solid. I. Low frequency range. *The Journal of the Acoustical Society of America* **28**(2): 168–178.

Biot MA. 1956b. Theory of propagation of elastic waves in a fluid-saturated porous solid. II. Higher frequency range. *The Journal of the Acoustical Society of America* **28**(2): 179–191.

Bindon HH. 1964. The design of snow samplers for Canadian snow surveys. *Proceedings of the Eastern Snow Conference* **21**: 23–28.

Bluestein LI. 1968. A linear filtering approach to the computation of the discrete Fourier transform. *Northeast Electronics Research and Engineering Meeting Record* **10**: 218–219.

Bogorodskii VV, Gavrilo VP, Nikitin VA. 1974. Characteristics of sound propagation in snow. *Soviet Physics Acoustics* **20**(2): 121–122.

Brittle K, Lines L. 2001. *Vibroseis deconvolution: an example from Pikes Peak, Saskatchewan*. CSEG Recorder May 2001, 28–35.

Brittle KF, Lines LR, Dey AK. 2001. Vibroseis deconvolution: a comparison of cross-correlation and frequency-domain sweep deconvolution. *Geophysical Prospecting* **49**(6): 675–686.

Buser O. 1986. A rigid frame model of porous media for the acoustic impedance of snow. *Journal of Sound and Vibration* **111**(1): 71–92.

Champoux Y, Allard JF. 1991. Dynamic tortuosity and bulk modulus in air-saturated porous media. *Journal of Applied Physics* **70**(4): 1975–1979.

Cummings WC, Holliday DV. 1983. Preliminary measurements of sound attenuation by snow over a model seal layer. *The Journal of the Acoustical Society of America* **74**(S1): S55.

Gibson B, Larner K. 1984. Predictive deconvolution and the zero-phase source. *Geophysics* **49**(4): 379–397.

Goodison BE, Ferguson HL, McKay GA. 1981. Measurement and data analysis. In *Handbook of Snow: Principles, Processes, Management and Use*, Gray DM, Male DH (eds). Pergamon Press: Toronto, Canada; 191–274.

Goodison BE, Metcalfe RA, Wilson RA, Jones K. 1988. The Canadian automatic snow depth sensor: a performance upgrade. *Proceedings of the Western Snow Conference* **56**: 178–181.

Goodison BE, Wilson B, Wu K, Metcalfe J. 1984. An inexpensive remote snow-depth gauge: an assessment. *Proceedings of the Western Snow Conference* **52**: 188–191.

Gubler H. 1981. An inexpensive snow depth gauge based on ultrasonic wave reflection from the snow surface. *Journal of Glaciology* **27**(95): 157–163.

Gubler H, Hiller M. 1984. The use of microwave FMCW radar in snow and ice research. *Cold Regions Science and Technology* **9**: 109–119.

Harrison C, Nielsen PL. 2004. Plane wave reflection coefficient from near field measurements. *The Journal of the Acoustical Society of America* **116**(3): 1355–1361.

Johnson DL. 1980. Equivalence between fourth sound in liquid He II at low temperatures and the Biot slow wave in consolidated porous media. *Applied Physics Letters* **37**(12): 1065–1067.

Johnson JB. 1982. On the application of Biot's theory to acoustic wave propagation in snow. *Cold Regions Science and Technology* **6**: 49–60.

Johnson DL, Plona TJ. 1982. Acoustic slow wave and the consolidation transition. *The Journal of the Acoustical Society of America* **72**(2): 556–565.

Johnson DL, Sen PN. 1981. Multiple scattering of acoustic waves with application to the index of refraction of fourth sound. *Physical Review B* **24**(5): 2486–2496.

Johnson DL, Koplik J, Dashen R. 1987. Theory of dynamic permeability and tortuosity in fluid-saturated porous media. *Journal of Fluid Mechanics* **176**: 379–402.

Johnson DL, Plona TJ, Scala C, Pasierb F, Kojima H. 1982. Tortuosity and acoustic slow waves. *Physical Review Letters* **49**(25): 1840–1844.

Jones HG, Pomeroy JW, Davies TD, Tranter M, Marsh P. 1999. CO_2 in Arctic snow cover: landscape form, in-pack gas concentration gradients, and the implications for the estimation of gaseous fluxes. *Hydrological Processes* **13**: 2977–2989.

Kennett BLN. 2001. *The Seismic Wavefield. Volume I: Introduction and Theoretical Development*. Cambridge University Press: Cambridge, UK.

Koh G, Mulherin ND, Hardy JP, Davis RE, Twombly A. 2002. Microwave interaction with snowpack observed at the cold land processes field experiment. *Proceedings of the Eastern Snow Conference* **59**: 251–254.

Lafarge D, Lemariner P, Allard JF, Tarnow V. 1997. Dynamic compressibility of air at audible frequencies. *The Journal of the Acoustical Society of America* **102**: 1995–2006.

Lee SM, Rogers JC. 1985. Characterization of snow by acoustic sounding: a feasibility study. *Journal of Sound and Vibration* **99**(2): 247–266.

Luck DGC. 1949. *Frequency Modulated Radar*. McGraw-Hill Book Company: New York.

Marshall HP, Koh G, Forster RR. 2004. Ground-based frequency-modulated continuous wave radar measurements in wet and dry snowpacks, Colorado, USA: an analysis and summary of the 2002-03 NASA CLPX data. *Hydrological Processes* **18**: 3609–3622.

Mathews JH. 1992. *Numerical Methods for Mathematics, Science and Engineering*. Prentice Hall: Englewood Cliffs, New Jersey.

Mewhort L, Bezdan S, Jones M. 2002. Does it matter what kind of vibroseis deconvolution is used? *CSEG Geophysics 2002 Conference Extended Abstracts:* 1–4.

Moore HM, Attenborough K, Rogers J, Lee S. 1991. In situ acoustical investigations of deep snow. *Applied Acoustics* **33**(4): 281–301.

Oura H. 1952a. Sound velocity in the snow cover. *Low Temperature Science. Series A, Physical Sciences* **9**: 171–178.

Oura H. 1952b. Reflection of sound at snow surface and mechanisms of sound propagation in snow. *Low Temperature Science. Series A, Physical Sciences* **9**: 179–186.

Pomeroy JW, Gray DM. 1995. *Snowcover accumulation, relocation and management*. National Hydrology Research Institute Science Report No. 7., National Hydrology Research Institute, Environment Canada: Saskatoon, Canada, 144.

Rabiner LR, Schafer RW, Rader CM. 1969. The chirp-z transform algorithm and its application. *IEEE Transactions on Audio Electroacoustics* **17**(2): 86–92.

Raichel DR. 2000. *The Science and Applications of Acoustics*. Springer-Verlag: New York; 17–18.

Robinson EA. 1957. Predictive decomposition of seismic traces. *Geophysics* **22**(4): 767–778.

Smith JL. 1965. *The elastic constants, strength, and density of Greenland snow as determined from measurements of sonic wave velocity*. Technical Report 167, Cold Regions Research and Engineering Laboratory: Hanover, NH, 1–18.

Smith N. 1969. *Determining the dynamic properties of snow and ice by forced vibration*. Technical Report 216, Cold Regions Research and Engineering Laboratory: Hanover, NH, 1–17.

Sommerfeld RA. 1982. A review of snow acoustics. *Reviews of Geophysics and Space Physics* **20**(1): 62–66.

Stove AG. 1992. Linear FMCW radar techniques. *IEE Proceedings-F: Radar and Signal Processing* **139**(5): 343–350.

Umnova O, Attenborough K, Shin H-C, Cummings A. 2005. Deduction of tortuosity and porosity from acoustic reflection and transmission measurements on thick samples of rigid-porous materials. *Applied Acoustics* **66**: 607–624.

Woo MK. 1997. *A Guide for Ground Based Measurement of the Arctic Snow Cover*. Climate Research Branch, Atmospheric Environment Service: Downsview, ON; 6.

Yankielun N, Rosenthal W, Davis RE. 2004. Alpine snow depth measurements from aerial FMCW radar. *Cold Regions Science and Technology* **40**: 123–134.

Zhekamukhov MK, Malkandueva LM. 2004. Propagation of elastic vibrations in snow. *Journal of Engineering Physics and Thermophysics* **77**(6): 1205–1212.